Low-Energy Break in the Spectrum of Galactic Cosmic Rays

A. Neronov,[1] D. V. Semikoz,[2] and A. M. Taylor[1]
[1]ISDC Data Center for Astrophysics, Ch.d'Ecogia 16, 1290, Versoix, Switzerland
[2]APC, 10 rue Alice Domon et Leonie Duquet, F-75205 Paris Cedex 13, France
(Received 10 September 2011; published 31 January 2012)

Measurements of the low-energy spectrum of Galactic cosmic rays (GCRs) by detectors on or near Earth are affected by solar modulation. To overcome this difficulty, we consider nearby molecular clouds as GCR detectors outside the Solar System. Using γ-ray observations of the clouds by the Fermi telescope, we derive the spectrum of GCRs in the clouds from the observed γ-ray emission spectrum. We find that the GCR spectrum has a low-energy break with the spectral slope hardening by $\Delta\Gamma = 1.1 \pm 0.3$ at an energy of $E = 9 \pm 3$ GeV. Detection of a low-energy break enables a measurement of GCR energy density in the interstellar space $U = 0.9 \pm 0.3$ eV/cm^3.

DOI: 10.1103/PhysRevLett.108.051105 PACS numbers: 98.70.Sa, 95.85.Pw, 98.38.−j

Introduction.—The spectrum of cosmic rays (CRs) with energies $E < 100$ GeV measured by CR detectors inside the Solar System [1–3] is not identical to the Galactic CR (GCR) spectrum due to the extinction of the low-energy CRs by the solar wind [4–6]. Uncertainties in the knowledge of properties of the solar wind, its termination shock, heliosheath, and heliotail introduce uncertainties in our knowledge of the GCR spectrum.

The only possibility to measure the GCR spectrum unaffected by the solar modulation is to consider nearby mass concentrations, like giant molecular clouds (GMCs) as natural CR detectors [7–10]. The nearest GMCs form the Gould Belt, a ringlike structure of diameter $\sim$1 kpc inclined at $\sim$20° to the Galactic plane [11,12]. CR-induced γ-ray emission from the Gould Belt clouds was previously detected by the COS-B gamma-ray telescope [13,14], the Energetic Gamma Ray Experiment Telescope [15,16], and the Large Area Telescope (LAT) on board the Fermi satellite [17,18].

The bulk of γ-ray emission from the GMCs is produced by GCR interactions. The GCR spectrum may be reconstructed by using the measured γ-ray spectrum from the clouds combined with the known relevant particle physics of pion production and decay [19,20] (a comparison of different codes for the calculation of pion production in pp interactions was recently done in Ref. [21]). In what follows, we report such a measurement.

Data selection and analysis.—Clouds from the Gould Belt span large angular sizes $\Theta \sim 1°$–$10°$. Most of these clouds lie in the Galactic plane, so that the γ-ray emission is superimposed on the diffuse Galactic emission. This makes the analysis of characteristics of cloud γ-ray emission difficult: The diffuse Galactic emission is variable on the angular scales comparable to Θ and has similar spectral characteristics. Clouds at high Galactic latitudes are separated from the Galactic plane. Analysis for these clouds can thus be done in a straightforward way. Taking this into account, we concentrate on the study of high Galactic latitude ($|b| > 10°$) clouds listed in Table I.

We use the LAT data collected between August 4, 2008 and July 15, 2011. We filter the data with Fermi SCIENCE TOOLS [22] (software version V9R23P1 and data selection P6_V11) using GTSELECT, GTMKTIME and GTBIN. We retain only γ-ray events (DATACLEAN events) at zenith angle $\leq 100°$. We use the aperture photometry method for the spectral analysis, by collecting the events from "source" regions and comparing the total number of counts in each source region with the number of background events, estimated from nearby "background" regions at the same Galactic latitude. The lists of source and background regions is given in Table I. The exposure is calculated by using the GTEXPOSURE tool.

Large regions occupied by the clouds contain point sources. Emission from the point sources is superimposed on the diffuse emission from the clouds. To subtract the point sources, we use the list of sources from the 2 yr exposure of LAT [23].

TABLE I. High Galactic latitude Gould Belt clouds considered in the analysis. l_s, b_s, and Θ_s are the coordinates of the center and radius of regions from which source counts are collected. l_b and b_b are the coordinates of the centers of 5° regions used for background estimation. Masses M (in units of $10^5 M_\odot$) and distances D (in parsecs) to the clouds are from Ref. [11].

Name	(l_s, b_s)	Θ_s	(l_b, b_b)	D	M
Perseus OB2	(159.28, −20.22)	4.0	(148.43, −19.91)	350	1.3
Taurus	(173.17, −14.70)	6.0	(185.96, −16.86)	140	0.3
Orion A	(212.23, −19.10)	4.0	(222.51, −23.47)	500	1.6
Orion B	(204.79, −14.15)	4.0	(220.92, − 22.29)	500	1.7
Mon R2	(213.79, −12.58)	1.5	(220.92, −22.29)	830	1.2
Chameleon	(300.42, −16.09)	5.5	(283.78, −15.88)	215	0.1
Rho Oph	(355.80, 16.63)	5.0	(4.73, 15.90)	165	0.3
R CrA	(0.60, −19.64)	3.0	(6.12, −22.35)	150	0.03
Cepheus	(108.54, 14.78)	6.0	(92.10, 13.34)	450	1.9

The point spread function of LAT becomes comparable to the size of the clouds at energies $\lesssim 0.3$ GeV for photons pair converted in the "front" layer of the LAT and at $\lesssim 0.7$ GeV for photons converted in the "back" layer. We use only front photons for the analysis between 0.3 and 0.7 GeV. We do not use the $E < 300$ MeV data.

Gamma-ray spectrum of the clouds.—All the clouds listed in Table I are detected as extended sources with LAT. The morphology of γ-ray emission follows the morphology of CO emission as inferred from the CO maps [11,24]. The γ-ray flux is proportional to the CO integrated intensity as expected if the flux scales as $F \sim M/D^2$ with M and D being the cloud mass and distance, respectively [7–10]. Images and spectra of individual clouds can be found in [25].

We verified that the spectra of individual clouds are consistent with each other and with the "local atomic hydrogen" component of diffuse Galactic emission derived in Ref. [26] (Fig. 1). This implies that all the high-latitude Gould Belt clouds are "passive" CR detectors, with no ongoing particle acceleration and no modification of CR propagation inside the clouds (i.e., the CR diffusion coefficient does not change significantly in the clouds [9]). The average spectrum of the clouds is shown in Fig. 1.

From Fig. 1, we see that the γ-ray spectrum exhibits a break at $\sim$2 GeV. Several explanations of this break can be considered: a break in the spectrum of CR nuclei or CR electrons or positrons or a break in the γ-ray production cross section.

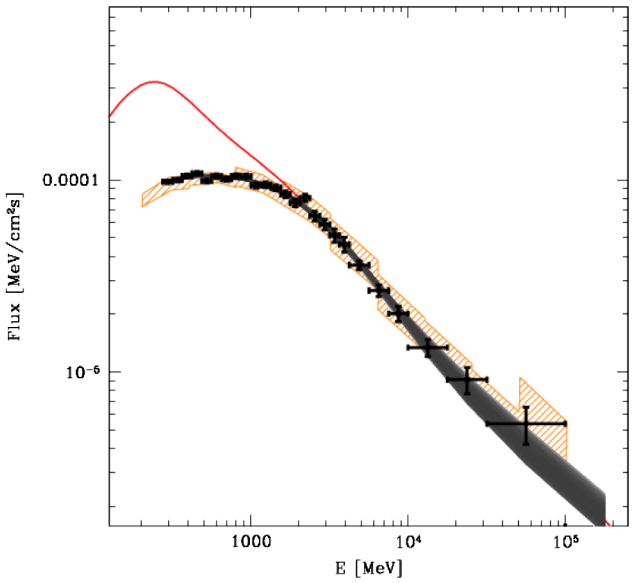

FIG. 1 (color online). Spectrum of diffuse γ-ray emission from high Galactic latitude GMCs. The red thin curve is the spectrum of γ-ray emission calculated by assuming a power-law CR spectrum. The orange hatched region is the "local atomic hydrogen" component from Ref. [26], renormalized by a factor of 23.7 to match the normalization of the GMC average spectrum. The gray-shaded area shows model spectra calculated by assuming a broken power-law GCR spectrum.

γ rays with energies $\sim$2 GeV are produced by protons with energies much higher than the pion production threshold, where the proton-proton interaction cross section grows logarithmically with energy. The break could also not be related to a feature in the electron bremsstrahlung cross section, since this also grows logarithmically at GeV energies. The most reasonable explanation for the $\sim$2 GeV feature is that it is related to a feature in the CR spectrum.

CR spectrum.—We have reconstructed the spectrum of CRs from the γ-ray spectrum by using the parametrized pion production spectra calculated in Ref. [19]. Figure 1 shows a comparison of the observed γ-ray spectrum with that produced by a power-law distribution of CR protons and nuclei. The spectrum produced by a power-law CR spectrum has a peak at $\sim$300 MeV, and the model overpredicts the γ-ray emission below $\sim$1 GeV. The sub-GeV flux could be suppressed if the GCR spectrum hardens below $\sim$10 GeV.

To find the details of the low-energy hardening, we model the spectrum as a broken power law $dN_{\rm CR}/dE \sim (E/E_{\rm Br})^{\Gamma_1}/[1 + (E/E_{\rm break})^{\sigma}]^{(\Gamma_2+\Gamma_1)/\sigma}$ with low and high energy slopes Γ_1 and Γ_2, break energy $E_{\rm break}$, and sharpness of the break σ. Assuming a negligible bremsstrahlung contribution, a satisfactory fit to the γ-ray spectrum is found, with $\chi^2/{\rm dof} = 23/21$, which corresponds to a 34% probability for model to be the proper description of the data. The range of model γ-ray spectra consistent (at 68% confidence level) with the GMC data is shown in Fig. 1.

The conclusion about the presence of a low-energy break in the CR spectrum is not altered if a non-negligible bremsstrahlung component is considered. The maximal bremsstrahlung component is produced when electrons (primary CR electrons and secondary electrons produced in interactions of CR nuclei) lose all their energy via bremsstrahlung before leaving the clouds. This could happen if electron diffusion through the clouds is slower than in the interstellar medium (ISM). This is not realized in the Gould Belt, but considering the maximal bremsstrahlung component allows an estimate of influence of bremsstrahlung-related uncertainties. Including the maximal bremsstrahlung component, we find a satisfactory fit ($\chi^2/{\rm dof} \simeq 24/21$), which is achieved with a sharper break in the CR spectrum, because bremsstrahlung contributes mostly to the lower-energy part of the spectrum at $E \lesssim 300$ MeV [9].

To obtain the estimates for $E_{\rm break}$, Γ_1, Γ_2, and σ, we follow Ref. [27]. Projections of the 68% confidence intervals for the model parameters onto $(E_{\rm break}, \sigma)$, $(E_{\rm break}, \Gamma_2)$, (Γ_1, Γ_2), and $E_{\rm break}, \sigma$ planes are shown in Fig. 2. The sharpness of the break, σ, is constrained from below. The best-fit model is the model of the form $dN_{\rm CR}/dE \sim (E^{-\Gamma_1}, E < E_{\rm Br}) \bigcup (E^{-\Gamma_2}, E > E_{\rm Br})$. The

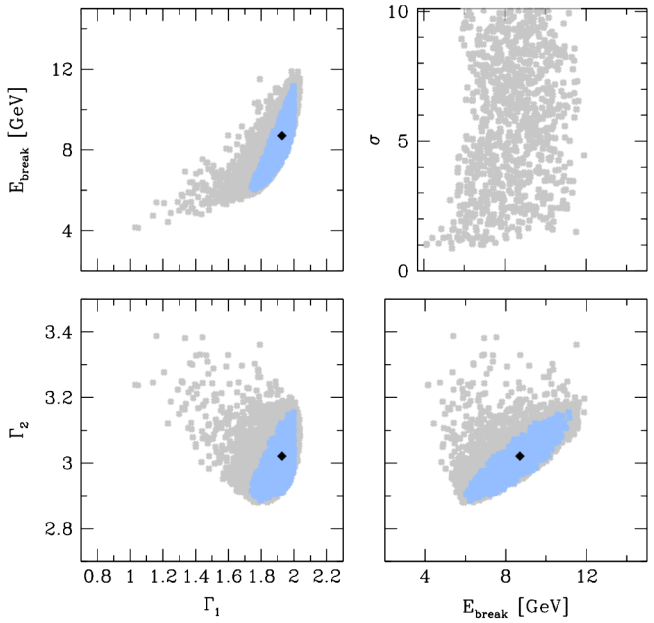

FIG. 2 (color online). 68% confidence ranges for $E_{\rm break}$, Γ_1, Γ_2, and σ parameters. The black dot shows the best fit. The light-blue-shaded region is for $\sigma \to \infty$, and the gray-shaded region is for finite σ.

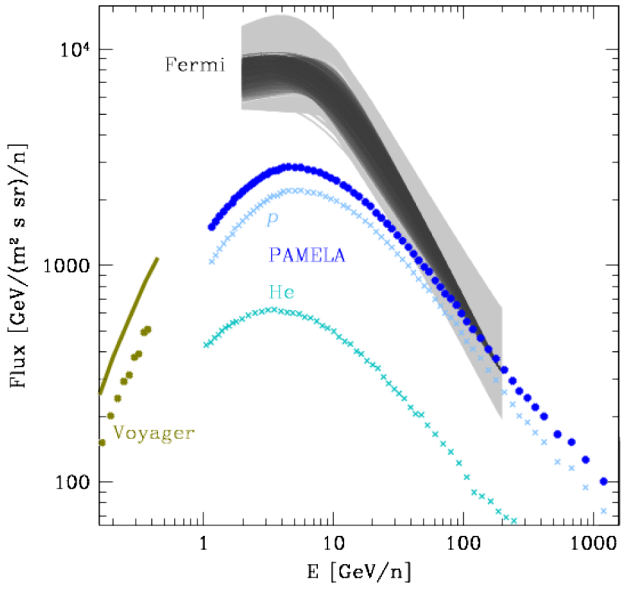

FIG. 3 (color online). Light gray: GCR spectrum inferred from the LAT observations. Dark gray: GCR spectrum inferred from the LAT observations with normalization fixed at 200 GeV to PAMELA. Thin data points are proton (light blue), helium (cyan), and the total (blue) CR spectrum measured by PAMELA [2]. Olive data points in the 0.1–0.35 GeV range are Voyager data for CR flux beyond the solar wind termination shock [3]. The solid curve is the GCR spectrum reconstructed from Voyager [3,6].

confidence regions for model parameters in the "sharp break" model are shown as light-blue shaded regions in Fig. 2. Projecting these regions onto coordinate axis, one finds $E_{\rm break} = 9 \pm 3$ GeV and $\Gamma_2 = 3.03 \pm 0.17$, $\Gamma_1 = 1.9 \pm 0.2$. Considering the model with the maximal bremsstrahlung component, one finds a reduced estimate for $\Gamma_1 = 1.7 \pm 0.2$. Leaving parameter σ free increases the error bars to $E_{\rm break} = 9^{+3}_{-5}$ GeV, $\Gamma_2 = 3.03^{+0.37}_{-0.18}$, and $\Gamma_1 = 1.9^{+0.2}_{-0.9}$.

The PAMELA Collaboration has reported a measurement of the CR spectrum in the range 50 GeV $< E <$ 200 GeV with the spectral slope of $\Gamma \simeq 2.85$ [2]. LAT measurements are mostly sensitive to the part of the CR spectrum below 200 GeV. The slope of the CR spectrum Γ_2 is consistent with the PAMELA measurement in the 50–200 GeV range. Below 50 GeV, the CR spectrum derived from Fermi measurement is still consistent with a power law down to $\simeq 10$ GeV, while the spectrum measured by the PAMELA deviates from the power law.

Contrary to the shape, the normalization of the GCR spectrum is more difficult to measure by using the γ-ray data. The problem here is the large uncertainty (by a factor of $\sim$2) of the amount of target material in the clouds. To remove this uncertainty, we normalize the CR flux above 200 GeV in the PAMELA data. This is justified because the effect of the heliospheric distortion at this energy is minor. The GCR spectrum normalized in this way is shown by the dark shaded curve in Fig. 3.

An alternative possibility to find the normalization of GCR spectrum is to infer the γ-ray emissivity per hydrogen atom which is determined by the CR density. Such a measurement relies on an estimate of the hydrogen column density from the CO maps using the CO-to-N_{H_2} conversion "X factor". Assuming $X = 1.8 \times 10^{20}$ cm^{-2} K^{-1} km^{-1} s [24], we derive the normalization of the CR spectrum shown by the light gray band in Fig. 3. A constant nuclear enhancement factor $\kappa \sim 1.5$–1.8, which accounts for the nuclear composition of the CR flux and of the interstellar medium, was assumed [28,29]. The statistical uncertainty of such a measurement ($\sim 10\%$) is much smaller than the systematic uncertainty related to uncertainty of the X factor [18] ($\sim 40\%$) and by the uncertainty of κ ($\sim 20\%$) [28,29]).

Discussion.—The LAT observation of the high Galactic latitude clouds from the Gould Belt shows that the steepening of GCR spectrum below $\sim$200 GeV persists down to $\sim$10 GeV. The PAMELA spectrum below $\sim$50 GeV deviates from the GCR spectrum derived from the LAT data. This could be attributed to the distortion of the GCR spectrum in the heliosphere. In the conventional modeling, the heliosphere is assumed to affect the CR flux only below $\sim$10 GeV, in the energy band where the solar modulation, or time variability of the flux, is observed [1]. However, the heliospheric effects might affect the CR spectrum up to TeV energies at which the gyroradius of CRs becomes comparable to the size of the heliosphere, $\sim$100 AU. At 50 GeV, the gyroradius is $R_L = E/eB \simeq 1[E/50\ \text{GeV}] \times [B/10\ \mu\text{G}]^{-1}$AU, comparable to the size of magnetic

structures in the outer heliosphere recently revealed by the Voyager spacecrafts [30]. The possibility that the heliosphere influences the CR flux at the energies higher than 10 GeV, which, though physically justifiable, needs to be further investigated. Residual influence of the heliosphere might be present up to still higher energies, ~1–10 TeV, at which the anisotropy of the CR flux in the direction toward and opposite of the heliotail is observed [31].

The GCR spectrum breaks by $\Delta\Gamma \simeq 1$ below ~10 GeV. Such a break was not reported before, although indications for the existence of a break, based on comparison of the CR data with GCR propagation models, were discussed [21,32,33]. A possibility of the existence of a break in the spectrum of CR electrons in the same energy range was recently discussed [34]. The main difference between our result and that of Refs. [21,32,33] is that we obtain a direct and model-independent measurement of the break, without any assumptions on the distribution of sources in the Galaxy and details of CR propagation. A potential uncertainty of our measurement is the possible effect of CR propagation in the clouds on the measured spectrum. The absence of cloud-to-cloud variations of the position of the break argues against such a possibility. Small cloud-to cloud variations might be detectable with deeper exposure by LAT.

The hard slope of GCR spectrum below the break, $\Gamma_1 \lesssim 2$, is important because it ensures a finite energy density of GCRs [5]. Upper limits on the GCR flux in the 0.1–0.35 GeV range were derived from the Voyager measurements [3,6] (Fig. 3). Combining the Voyager constraint with the LAT measurements, we derive a measurement of the GCR energy density: $U_{\rm CR} = 0.9 \pm 0.3$ eV/cm^3. Such an energy density is in equipartition with the energy density of magnetic fields $U_B \simeq 1[B/6\ \mu{\rm G}]^{1/2}$eV/cm^3 and turbulent motions $U_{\rm turb} \simeq 1[n_{\rm ISM}/1\ {\rm cm}^{-3}] \times [v_{\rm turb}/20\ {\rm km/s}]^2$eV/cm^3 of the ISM with density $n_{\rm ISM}$ and turbulent velocity $v_{\rm turb}$, a fact which points to a physical coupling between the three ISM components.

The detection of a low-energy break introduces a new energy scale into the CR physics. Taking into account that the new energy scale is not far from the ''natural'' scale of proton rest energy m_pc^2, we have tested a possibility that the new scale could be reduced to m_pc^2 if the broken power-law model of the CR spectrum is changed to an alternative model of the form $dN_{\rm CR}/dE \sim \beta^{p_1}\mathcal{R}^{p_2}$, where β and $\mathcal{R}$ are CR velocity and rigidity, respectively. Such a shape of the GCR spectrum does not have additional scale except for m_pc^2. We find that such a GCR spectrum is inconsistent at $>4\sigma$ with the LAT data, with the best-fit value $\chi^2/{\rm dof} > 3$ for 23 dof.

A change of the CR spectral slope might be related to the physics of CR sources (e.g., characteristic maximal, minimal, or break energy of CRs produced by a source population [21,32,33] or injected by annihilation or decay of dark matter) or to a change of the propagation for CRs (e.g., transition from the convective to diffusive regime [8,32] or change in the energy dependence of the diffusion coefficient [32,35] and/or diffusive reacceleration possibly combined with an intrinsic break in the source spectra [33,35]).

A low-energy cutoff in the source spectra could occur, e.g., if the lower-energy particles are trapped by magnetic fields inside the sources. CRs of energies ~10 GeV propagate through the Galaxy in a diffusive way by scattering on turbulent inhomogeneities in ISM. A feature in the turbulence spectrum at a length scale λ_T might produce a break in the CR spectrum at an energy at which the Larmor radius $R_L = E_{\rm CR}/eB$ (B is the magnetic field in the ISM) is comparable to λ_T. Scattering and/or absorption of the lower-energy CRs would be determined by the energy-independent geometrical cross section of the smallest ISM inhomogeneities. In such a model, measurement of the break energy $E_{\rm break} \sim 10$ GeV implies the detection of a feature in the distribution of inhomogeneities of ISM at the length scale $\lambda_T \sim E_{\rm break}/eB \sim 1$ AU.

Suppression of the low-energy CR flux might also occur through efficient CRs interactions with the ISM on the time scale of proton-proton interactions $t_{pp} \simeq 3 \times 10^7[n_{\rm ISM}/1\ {\rm cm}^{-3}]^{-1}$ yr. During this time, CRs could spread over a region of the size $R(E) \lesssim \sqrt{D(E)t_{pp}} \sim 1[E/1\ {\rm GeV}]^{0.3}[n_{\rm ISM}/1\ {\rm cm}^{-3}]^{-1/2}$ kpc around a CR source [assuming $D(E = 1\ {\rm GeV}) \sim 10^{28}$ cm^2/s for the CR diffusion coefficient]. If the distance to the nearest GCR accelerator is in the kiloparsec range, energy losses would efficiently remove CRs with energies below several GeV from the locally observable GCR flux. This mechanism of suppression of the GCR flux could work only if the last episode of injection of GCR within a 1 kpc volume occurred not later than $t_{\rm GCR} \sim t_{pp} \sim 3 \times 10^7$ yr ago. Remarkably, this estimate is close to the age of the Gould Belt, which was formed in an explosive event some $t_{\rm GB} \simeq 3 \times 10^7$ yr ago [12].

This work was supported by the Swiss National Science Foundation Grant No. PP00P2_123426/1. We are grateful to M. Audard, A. Carmona, and F. Aharonian for discussions of the subject.

[1] Y. Shikaze *et al.*, Astropart. Phys. **28**, 154 (2007).
[2] O. Adriani *et al.*, Science **332**, 69 (2011).
[3] W. R. Webber and P. R. Higbie, J. Geophys. Res. **114**, A02103 (2009).
[4] E. N. Parker, Phys. Rev. **110**, 1445 (1958).
[5] T. K. Gloeckler and J. R. Jokipii, Astrophys. J. **148**, L41 (1967).
[6] V. Florinski and N. V. Pogorelov, Astrophys. J. **701**, 642 (2009).
[7] F. A. Aharonian, Astrophys. Space Sci. **180**, 305 (1991).
[8] F. A. Aharonian, Space Sci. Rev. **99**, 187 (2001).
[9] S. Gabici, F. A. Aharonian, and P. Blasi, Astrophys. Space Sci. **309**, 365 (2007).

[10] S. Casanova *et al.*, Publ. Astron. Soc. Jpn. **62**, 769 (2010).
[11] T. M. Dame *et al.*, Astrophys. J. **322**, 706 (1987).
[12] C. A. Perrot and I. A. Grenier, Astron. Astrophys. **404**, 519 (2003).
[13] P. A. Caraveo *et al.*, Astron. Astrophys. **91**, L3 (1980).
[14] J. B. G. M. Bloemen *et al.*, Astron. Astrophys. **139**, 37 (1987).
[15] S. W. Digel, S. D. Hunter, and R. Mukherjee, Astrophys. J. **441**, 270 (1995).
[16] S. W. Digel, E. Aprile, S. D. Hunter, R. Mukherjee, and F. Xu, Astrophys. J. **520**, 196 (1999).
[17] A. Okumura and T. Kamae, arXiv:0912.3860.
[18] A. A. Abdo *et al.*, Astrophys. J. **710**, 133 (2010).
[19] T. Kamae *et al.*, Astrophys. J. **647**, 692 (2006).
[20] S. R. Kelner, F. A. Aharonian, and V. V. Bugayov, Phys. Rev. D **74**, 034018 (2006).
[21] I. Cholis *et al.*, arXiv:1106.5073.
[22] http://fermi.gsfc.nasa.gov/ssc/data/analysis/scitools/
[23] http://fermi.gsfc.nasa.gov/ssc/data/access/lat/2yr_catalog/ (2011).
[24] T. M. Dame, D. Hartmann, and P. Thaddeus, Astrophys. J. **547**, 792 (2001).
[25] See Supplemental Material at http://link.aps.org/supplemental/10.1103/PhysRevLett.108.051105 for images and spectra of individual clouds listed in Table I.
[26] A. A. Abdo *et al.*, Phys. Rev. Lett. **104**, 101101 (2010).
[27] M. Lampton, B. Margon, and S. Bowyer, Astrophys. J. **208**, 177 (1976).
[28] T. Delahaye *et al.*, Astron. Astrophys. **531**, A37 (2011).
[29] M. Mori, Astropart. Phys. **31**, 341 (2009).
[30] M. Opher *et al.*, Astrophys. J. **734**, 71 (2011).
[31] M. Amenomori, in Proceedings of the Thirty-second ICRC, Beijing, 2011 (unpublished), ID0361.
[32] I. V. Moskalenko *et al.*, Astrophys. J. **565**, 280 (2002).
[33] R. Trotta *et al.*, Astrophys. J. **729**, 106 (2011).
[34] A. W. Strong, E. Orlando, and T. R. Jaffe, Astron. Astrophys. **534**, A54 (2011).
[35] A. Putze, Astron. Astrophys. **526**, A101 (2011).